Investigating mediastinal lymph node stations segmentation on thoracic CT following experts guidelines

D. Sarrut, L. Claude, S. Rit, R. Pinho, G. Pitson, R. Lynch

Investigating mediastinal lymph node stations segmentation on thoracic CT following experts guidelines

D. Sarrut[1,2], L. Claude[2], S. Rit[1,2], R. Pinho[1,2], G. Pitson[3], R. Lynch[3]

(1) Université de Lyon, CREATIS; CNRS UMR5220; Inserm U1044 ; France
(2) Department of Radiation Oncology, Centre Léon Bérard, Lyon, France
(3) Department of Radiation Oncology, Andrew Love Cancer Centre, Barwon Health, Geelong, Australia.

Abstract. In radiation therapy, accurate delineation of mediastinal lymph node stations on thoracic CT is essential for both prognostication and treatment delivery. We propose an original approach based purely on geometrical considerations, without using grey levels, that follow the reference guidelines and attempt to replicate the delineation undertaken manually by the experts. The proposed method is a greedy process based on fuzzy relative position constraints. It progressively refines an initial region towards the target by using a set of predefined anatomical structures. Experiments were conducted with two CT images that were manually segmented by experts. Average Dice Similarly Coefficient between segmented and references stations was close to 77%. This fast method (30 sec) could potentially assist the expert, for example in detecting situations where the guidelines are not strictly followed. To our knowledge, this is the first time such an approach has been proposed for this problem.

1 Introduction

Mediastinal and hilar lymph node involvement often occurs in lung cancer. A reference definition of lymph node station anatomy was recently updated by the IASLC Lung Cancer Staging Project. Such a definition is intended to be an internationally agreed framework that would allow precise and uniform determination of lymph node status by centres around the globe. This new map [13] contains important changes to the previously used Mountain-Dresler [11] and Naruke maps [12].

In radiation therapy, lymph node stations are sometimes included in the target volume, but there is currently no consensus on whether to electively irradiate uninvolved mediastinal nodal regions [4,6]. However, the accurate delineation of node regions on thoracic CT is essential for both prognostication and treatment delivery. In 2005, Chapet et al [2] published an atlas from the University of Michigan which defined the mediastinal nodal stations for lung cancer on CT images. This atlas has been superseded by the new IASLC lymph node. Lynch et al [9] have recently published a CT atlas, based on the new IASLC lymph node map.

The descriptors for the nodal map are based on anatomical structures within the mediastinum. The mediastinal nodal stations are numbered from their superior to inferior (SI) location, starting with the supraclavicular stations 1R and 1L (R for Right and L for Left), superior mediastinal : 2R, 2L, 3A, 3P, 4R, 4L (A for Anterior, P for Posterior), aortic: 5 and 6, inferior mediastinal : 7-9, hilar, lobar and (sub)segmental : 10-14 (figure 1). Each station is described according to the surrounding anatomical structures, such as aorta, carina, trachea, various vessels, etc. The limits and boundaries between the stations are indicated. Some geometrical constructions are defined to assist in delineating some nodal stations : for example, the boundary between 2R and 2L is defined by a vertical line passing tangentially along the left lateral tracheal border.

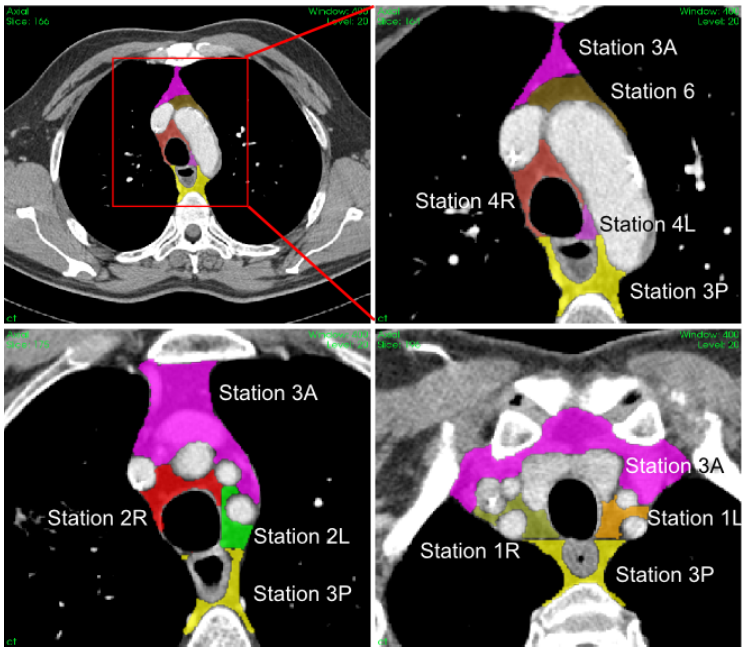

Fig. 1. Examples of mediastinal stations delineated on a thoracic CT.

The delineation of nodal stations is performed manually, on an intravenous (IV) contrasted thoracic CT, on a slice by slice basis. The guidelines make use of natural orientations, referring to AP, SI and LR axis. Manual delineation of all the normal anatomical structures and lymph node stations within the mediastinum is a time consuming process. The inter-patient anatomical variability and the inter-experts variability are high [7].

Several articles have described segmentation methods for nodal delineation, e.g. [5,10], but not for stations. Lu et al. [8] described a method to determine

cuboid (parallelepiped) regions that encompass stations. Other works proposed head and neck lymph node station segmentation for radiation therapy planning. Commowick et al. [3] proposed an atlas-based method that used deformable image registration to deform reference lymph station contours against current patient image. Good results were obtained but due to the high variability of the stations and the presence of low-contrast regions, this process can be further improved.

To our knowledge, no published work has been designed for the automated delineation of mediastinal lymph node stations. We propose an original approach, different from atlas-based and grey-level-based segmentation methods, based purely on geometrical considerations that follow the reference guidelines and attempt to replicate the delineation of nodal stations undertaken manually by the experts.

2 Method

Principles. We investigated the feasibility of segmenting the stations by following their geometrical description in the guidelines [13,9], e.g. their relative positions to surrounding anatomical structures. We tried to reproduce this description and thus made no use of the grey levels of the CT image. The proposed process was the same for all stations. It started from an initial 3D binary image S, called the support. Then, a greedy and subtraction based process was applied: at each step i some pixels were removed from the current support S_i according to anatomical and geometrical constraints. The result formed the new current support S_{i+1}; no pixels were added from step to step. After all the constraints had been applied, the last support $S_{i=last}$ was the resulting station. Geometrical constraints were defined according to identified anatomical structures that were considered to be available in the form of 3D binary images.

Relative Position (RP) constraints. We define an RP operator that considered the current support S, an object A, an angular relationship α (such as "at left of A") and a threshold t. The operator removed from S all pixels that did not fulfill the orientation relation α according to a tolerance threshold t. Following the framework of [1], the orientation relation was determined by a fuzzy map $\mu_{\alpha,A}(x)$, with $x \in S$ a pixel position, that gives at x the degree of validity of the relation. We chose the same functions to that in [1] : the fuzzy value at a given point x was a linear function $\mu_{\alpha,A}(x) = max\left(0, 1 - \frac{2\beta_{min}(x)}{\pi}\right)$ of the minimal value $\beta_{min}(x) = min_{y \in A}\beta(x,y)$ among all the angles between the considered direction $\overrightarrow{d_\alpha}$ and each point y in the object $\beta(x,y) = \arccos\frac{\overrightarrow{yx}.\overrightarrow{d_\alpha}}{||\overrightarrow{yx}||}$ and $\beta(x,x) = 0$. The fuzzy landscape was computed with the proposed fast propagation algorithm, in two passes with a neighborhood of radius 2. Once the fuzzy map was obtained, the threshold t was used to create a binary image $RP_S(A,\alpha,t)$ in which the pixel value 1 indicated at which pixel position the relationship was acceptable. If a RP contained "Not to", $1 - \mu_{\alpha,A}(x)$ was considered instead. The last step

performed the boolean intersection between this binary image and the support: $S_{i+1} = S_i \cap RP_S(A, \alpha, t)$. RP can be used in 3D (with two angles $\alpha = (\alpha_1, \alpha_2)$) or in 2D, slice by slice. We used 3D or 2D approaches according to what was indicated in the guidelines.

As we wanted to stay as close as possible to the human readable description used in the guidelines, we consider natural orientations such as "Left to" or "Not Anterior to". This lead to 12 different orientations, combined or not with the "Not To" operator. For example, if the nodal station was indicated to be "at Left to the Aorta", all of the pixels that were not to the left of the Aorta were removed. To further illustrate this point, if the nodal station was "Not Anterior to the Brachiocephalic Vein", the voxels that were anterior to this structure were discarded from the current support. Figure 2 illustrates this process.

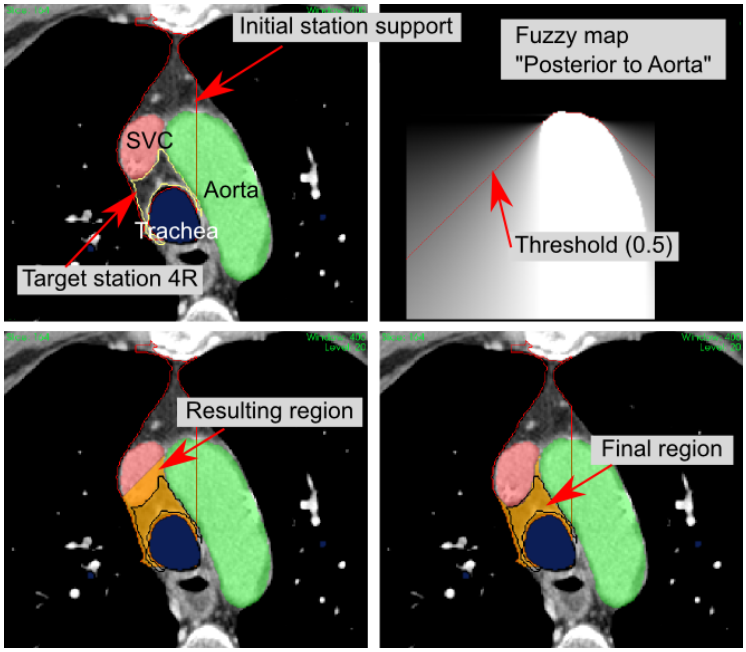

Fig. 2. Illustration of one RP operation. Initial support S_i of station 4R is shown in red contour top/left. RP is "Posterior to Aorta". The corresponding fuzzy map is shown top/right, with the threshold $t = 0.5$. Next resulting support S_{i+1} is bottom/left. Final station after other RP is bottom/right. In all images, the reference contour of target station 4R is drawn in yellow and black.

When considering several successive RP operations, fuzzy maps could be merged and a single threshold value could be used. However, we decided not to combine fuzzy maps but rather consider successive operations, like in the

guidelines. It requires one threshold by operation, but allows a better control and potential visual feedback to the user. Moreover, as the support size decreased after each RP operation, it decreased the computation time because the fuzzy maps should only be computed on the current support S_i.

Geometrical constraints. In the guidelines, in addition to the RP constraints, other geometrical descriptions were also given, such as *"The boundary between stations 2R and 2L is defined by a vertical line passing tangentially along the left lateral tracheal border"*. We translated this description into algorithms that will not be described here. Table 1 describes the anatomical structures used in the process. Some of them were obtained automatically according to methods already available by our team. The others have been delineated manually by the experts. It should be noted that the majority of structures do not need to be delineated entirely on all slices because they are only used as references within selected regions. The accuracy in the segmentation is also not a critical point because only some parts of the structures are used. For example only the anterior part of the vertebral body is use required to be delineated accurately whereas the posterior aspect can be demarcated roughly.

Initial mediastinum and stations supports. The first step consists of determining the initial support S_0 for all stations. This is done by determining a common mediastinal support automatically computed by considering areas to the left of the right lung and to the right of the left lung with the RP operator. Then we determined cuboid regions corresponding to LR, AP and SI limits of each stations, similarly to [8]. Stations were then segmented starting from superior (1R 1L), to inferior (S6), in the guidelines order. Each station description contains around 4 to 8 RP operators and geometrical limits. The different threshold values, t, were manually defined. The total process was composed of about 130 different operations (including RP).

3 Experiments and results

We tested the approach with the delineated atlases of two patients, performed by radiation oncologists in a consensus framework [9], with the new IASLC stations definition [13]. CT were acquired with IV contrast with a resolution of $0.66 \times 0.66 \times 1.5$ mm. Each atlas contains the delineation of stations (1R, 1L, 2R, 2L, 3A, 3P, 4R, 4L, 5, 6) and the anatomical structures. Delineations for other patients are in progress. We used the Dice Similarity Coefficient $DSC(A, B) = \frac{2A \cap Bt}{A+B}$ to quantify the overlap between two 3D structures A and B. We depict in table 2 the evolution of DSC between the reference station and 1) the initial whole mediastinal region S_0, 2) the initial station's parallelepiped supports S_1 and 3) the final result S_{final}.

Globally, we observed an overlap greater than 70%. There was an exception for stations 1L, p1: in that specific case we observed that the reference delineation proposed by the expert did not perfectly follow the guidelines. On some slices

	S1R	S1L	S2R	S2L	S3A	S3P	S4R	S4L	S5	S6
Bony structures										
Rib Cage					X					
Sternum	X	X	X	X	X					
CricoidCartilag (P)	X	X								
ClavicleRight	X									
ClavicleLeft		X								
FirstRibRight	X									
FirstRibLeft		X								
Artery & Veins										
Aorta			X	X		X	X	X		X
AorticArch								X	X	X
AscendingAorta					X				X	
DescendingAorta									X	
VertebralArtery	X	X				X				
SubclavianArteryRight	X		X	X	X	X				
SubclavianArteryLeft		X	X	X	X	X				
CommonCarotidArteryLeft			X	X	X					
CommonCarotidArteryRight			X	X	X					
LeftPulmonaryArtery								X	X	
MainPulmonaryArtery									X	
BrachioCephalicArtery			X	X	X					
BrachioCephalicVein			X	X			X			X
AzygousVein						X	X			
SVC (Superior Vena Cava)					X		X			X
LowerBorderAzygousVein							X			
Others										
ScaleneMuscleAnt		X								
Esophagus						X				
Trachea	X	X			X		X	X		
Thyroid	X	X	X	X		X				

Table 1. List of anatomical structures used by station. Cricoid cartilage is marked with a P, because only a point corresponding to the inferior limit of this structure is needed, not the entire contour. In addition to these structures, the patient contour, and the right and left lungs are also used.

(4 slices for 1L), posterior borders of the stations should be delimited with the most anterior point in the right and left lung. This was not the case in the expert contour, but well described by the proposed algorithm. After correction of the reference delineation for 1R and 1L, DSC rose to greater than 80%. We decided to keep this situation in order to illustrate the interest in trying to strictly follow guidelines.

4 Discussion and conclusion

The results, although limited, show that interesting segmentation can be obtained, with a mean overlap almost equal to 77%. The proposed methodology has the advantage of following guidelines in a natural way and is fast because it only considers binary images with decreasing support sizes from step to step : about 30 sec using a conventional workstation (2.6 Gz). One limitation is the need to have one threshold value for each RP (but the same for all patients). These parameters do not appear to be very sensitive due to the limited dataset

Stations	p1			p2		
	Med.	Init.	Final	Med.	Init.	Final
Station 1R	28.2%	42.1%	73.0%	24.1%	37.3%	70.4%
Station 1L	35.8%	50.1%	67.3%	27.9%	44.4%	70.3%
Station 2R	27.1%	43.3%	75.0%	25.8%	42.7%	75.8%
Station 2L	24.1%	35.6%	74.0%	25.8%	40.3%	70.5%
Station 3A	42.8%	48.6%	85.3%	33.5%	39.4%	79.8%
Station 3P	29.1%	52.2%	80.0%	33.6%	63.1%	79.2%
Station 4R	28.6%	50.0%	86.1%	30.6%	56.1%	83.1%
Station 4L	13.0%	20.1%	73.5%	9.1%	26.8%	74.0%
Station 5	20.7%	29.1%	84.5%	44.6%	63.6%	77.4%
Station 6	16.0%	22.8%	84.9%	17.8%	23.3%	73.5%

Table 2. For each station, Dice Similarity Coefficients between reference station and mediastinal support S_0 ("Med."), cuboid initial support S_1 ("Init"), and final result S_{final} ("Final").

but may become more accurate if the dataset was larger. Another limitation is that the guidelines are sometimes hard to translate into algorithmic operators. However, this could be view as an advantage because the proposed method could potentially point out ambiguities or gaps in the guidelines. If there was demonstrated uncertainty in the guidelines, this could be investigated. A further limitation of this method is the requirement to have several anatomical structures delineated prior to segmentation. However, we argue that such structures are only needed in part and segmentation could be performed automatically with conventional methods, for example with atlas or region-growing. The description of the exact part of all structures that should be delineated is also an important work that can help experts.

Our aim with this technique is not to fully replace manual delineation, but rather provide tools that can help delineations and potentially improve consistency. Several applications can be imagined. First, the resulting automated regions can be proposed to the expert as a starting point to the manual process. It is still to be determined if this could result in efficiency gains. A second application could be to compare manual delineations with the automated one in order to assist the experts in following all the guidelines. If a database of cases were available, differences between manually versus automated segmented regions could reveal potential ambiguities or deficiencies of the descriptions in the guidelines. Segmented stations could also be useful for node segmentation, to automatically label found nodes.

Regarding the proposed method, we only considered orientation relations (RP), but other topological or distance relations could be used. If a larger dataset was available, threshold values could be learnt from the delineations performed by the experts, instead of being manually defined. Future works will study such a learning approach.

We investigated here an automated method that follows the expert's guidelines for delineating mediastinal nodes stations on CT images. To our knowledge, this is the first time such an approach has been proposed for this problem. The

preliminary results are promising and will hopefully lead to further developments with a larger dataset.

References

1. Bloch, I.: Fuzzy relative position between objects in image processing: a morphological approach. IEEE Transactions on Pattern Analysis and Machine Intelligence 21(7), 657–664 (1999)
2. Chapet, O., Kong, F.M., Quint, L.E., Chang, A.C., Ten Haken, R.K., Eisbruch, A., Hayman, J.A.: CT-based definition of thoracic lymph node stations: an atlas from the University of Michigan. International Journal of Radiation Oncology, Biology, Physics 63(1), 170–8 (2005)
3. Commowick, O., Gregoire, V., Malandain, G.: Atlas-based delineation of lymph node levels in head and neck computed tomography images. Radiotherapy and oncology : journal of the European Society for Therapeutic Radiology and Oncology 87(2), 281–9 (2008)
4. Fernandes, A.T., Shen, J., Finlay, J., Mitra, N., Evans, T., Stevenson, J., Langer, C., Lin, L., Hahn, S., Glatstein, E., Rengan, R.: Elective nodal irradiation (ENI) vs. involved field radiotherapy (IFRT) for locally advanced non-small cell lung cancer (NSCLC): A comparative analysis of toxicities and clinical outcomes. Radiotherapy and oncology : journal of the European Society for Therapeutic Radiology and Oncology 95(2), 178–84 (2010)
5. Feuerstein, M., Deguchi, D., Kitasaka, T., Iwano, S., Imaizumi, K., Hasegawa, Y., Suenaga, Y., Mori, K.: Automatic mediastinal lymph node detection in chest CT. Proceedings of SPIE pp. 72600V–72600V–11 (2009)
6. Kelsey, C.R., Marks, L.B., Glatstein, E.: Elective nodal irradiation for locally advanced non-small-cell lung cancer: it's called cancer for a reason. International journal of radiation oncology, biology, physics 73(5), 1291–2 (2009)
7. Kepka, L., Bujko, K., Garmol, D., Palucki, J., Zolciak-Siwinska, A., Guzel-Szczepiorkowska, Z., Pietrzak, L., Komosinska, K., Sprawka, A., Garbaczewska, A.: Delineation variation of lymph node stations for treatment planning in lung cancer radiotherapy. Radiotherapy and Oncology 85(3), 450–5 (2007)
8. Lu, K., Higgins, W.E.: Semi-automatic central-chest lymph-node definition from 3D MDCT images. In: Karssemeijer, N., Summers, R.M. (eds.) SPIE Medical Imaging 2010: Computer-Aided Diagnosis. vol. 7624 (2010)
9. Lynch, R., Claude, L., Pitson, G., Sarrut, D.: CT Atlas for the New International Lymph Node Map: A Radiation Oncologists Perspective. Practical Radiation Oncology to appear (2012)
10. Maleike, D., Fabel, M., Tetzlaff, R., Tengg-kobligk, H.V.: Lymph node segmentation on CT images by a shape model guided deformable surface method. In: SPIE Medical Imaging (2008)
11. Mountain, C.F., Dresler, C.M.: Regional Lymph Node Classification for Lung Cancer Staging. Chest 111(6), 1718–1723 (1997)
12. Naruke, T., Suemasu, K., Ishikawa, S.: Lymph node mapping and curability at various levels of metastasis in resected lung cancer. J. Thorac. Cardiovasc. Surg. 76(6), 832–839 (1978)
13. Rusch, V.W., Asamura, H., Watanabe, H., Giroux, D.J., Rami-Porta, R., Goldstraw, P., Others: The IASLC lung cancer staging project: a proposal for a new international lymph node map in the forthcoming seventh edition of the TNM classification for lung cancer. Journal of Thoracic Oncology 4(5), 568 (2009)